

Turbulent transport studies in the JET edge plasmas in limiter configuration

I García-Cortés[†], R Balbín[†], A Loarte[‡], J Bleuel[§], A Chankin, S J Davies, M Endler[§], S K Ereints^{||}, C Hidalgo[†], G F Matthews, B van Milligen[†] and H Thomsen[§]

JET Joint Undertaking, Abingdon, Oxfordshire, OX14 3EA, UK

[†] Asociacion EURATOM-CIEMAT, 28040 Madrid, Spain

[‡] EFDA CSU-Garching, Max-Planck-Institut für Plasmaphysik, D-85748 Garching bei München, Germany

[§] Max-Planck-Intitut für Plasmaphysik, EURATOM Association, 85740 Garching, Germany

^{||} EURATOM/UKAEA Fusion Association, Culham Science Centre, Abingdon, Oxfordshire OX14 3DB, UK

Received 16 October 1999, in final form 17 January 2000

Abstract. Electrostatic turbulence has been investigated in the plasma boundary region of the JET tokamak. The normalized fluctuation levels are in the range of 10–20% at the plasma radius where the poloidal velocity of the fluctuation reverses sign. In limiter plasmas, the $E \times B$ turbulent transport can account for a significant part of the total particle and energy losses. Three regions in the power spectra of the fluctuations with different frequency dependences have been found. The spectral region with power decay close to $1/f$ has been identified in the frequency range where the turbulent flux, which comes in bursts, is dominant. This result could be an indication of transport close to instability thresholds.

1. Introduction

Evidence for anomalous transport produced by electrostatic fluctuations in the plasma boundary region of tokamak experiments has been reported [1–3]. Initial work on the Caltech [1] and PRETEXT [4] tokamaks found levels of electrostatic fluctuation driven transport that were large enough to explain the observed anomalous losses of particles and energy. Subsequently, other tokamaks (TEXT [2], ISX-B [5], TOSCA [6], DITE [7]), stellarators (W7-AS [8]) and reversed field pinch (RFP [9]) confirmed these results. From all these experiments it appears that the turbulence induced fluxes can account for a large part of the anomalous particle and energy losses observed in the edge plasmas of fusion devices. The free energy sources responsible for edge plasma turbulence have not been fully identified yet [10]. However, a few systematic turbulent transport studies have been carried out in large devices. Turbulence in OH-, L- and H-mode regimes has been investigated previously in the DIII-D tokamak [11, 12], where edge turbulent particle transport seems to be responsible for most of the anomalous particle losses. Here poloidal asymmetries are taken into account to explain the fact that the turbulent particle flux at the outboard mid-plane exceeds the particle flux from a local transport model.

Recently, a study of the self-similarity properties of the fluctuations has led to very similar values of the self-similarity parameter for different devices [13], which supports the view that plasma turbulence and the associated turbulent transport display universality. It has

also been found that the fluctuation power spectra show the same functional dependence for different devices over a wide frequency range [14]. This could be an indication of the edge plasma turbulence evolving into a critical state, independent of the device size and plasma characteristics.

In this paper, we present results of electrostatic fluctuation measurements and calculations of the fluctuation-driven $E \times B$ particle transport in the JET boundary plasma using a fast reciprocating Langmuir probe array. This work was motivated by the need to understand the importance of the particle losses that are driven by the electrostatic turbulence in the global plasma parameters in large devices like JET, and what physical processes are responsible for the structure of the boundary plasma turbulence.

The remainder of this paper is outlined as follows. In section 2, the reciprocating probe array, the characteristics of the shots used in these experiments and the description of the fluctuation analysis techniques are described. In section 3, the general characteristics of the main turbulence parameters for limiter plasmas are shown. In section 4, the role of turbulent transport in the global particle/energy confinement is discussed. In section 5, the behaviour of power spectra for fluctuating quantities, as well as the identification of different frequency ranges and the comparison between the $1/f$ region and the spectral turbulent flux function are presented. Finally, we draw conclusions and present plans for further measurements in section 6.

2. Description of the experiment

The experiments reported in this paper were carried out in the Joint European Torus (JET Gas-Box pumped divertor) [15] boundary plasmas. The plasmas were produced in limiter and X-point magnetic configurations, although the analysis presented in this paper concentrates on the limiter phase. The geometric parameters of these plasmas are $R = 2.95$ m, $a = 1.04$ m $b/a = 1.3$.

The turbulent particle transport has been studied in the JET plasma boundary with a specially adapted Langmuir probe array [16]. Nine tips on the new probe head have been arranged in three groups of three. Two of them are at the same poloidal position, being separated radially by 0.8 cm. The third is located radially at the same position as the innermost group of tips (out of the previous two) but separated poloidally by 1.5 cm. The details of the probe head are shown in figure 1. This experimental set-up provides measurements of both the radial and poloidal structure of fluctuations. The system is installed in octant 5, on the top of the machine ($R = 3.253$ m) and the surface matches the plasma shape. The reciprocating probe insertion velocity is typically 1 m s^{-1} .

In every group of three tips the time-averaged ion saturation current (I_{sat}), floating potential (V_f) and their fluctuations (I_{sat} , V_f) are measured. A voltage ramp, with a sweep frequency of 0.1 kHz, is used in one of the group of tips in order to obtain the electron temperature (T_e). The edge plasma density (n_e) is determined from the measured T_e and I_{sat} ($I_{\text{sat}} \propto n_e T_e^{1/2}$), assuming the sheath boundary condition and $T_e = T_i$. Two poloidally spaced probes allow the poloidal electric field (E_θ) to be estimated from the difference in V_f , using the relation between floating and plasma potential (V_p): $V_f = V_p - 3kT_e$ and assuming T_e poloidally invariant. The inferred turbulent particle flux is $\Gamma_r = \langle \tilde{n} \tilde{E}_\theta \rangle / B_T$ [17], where the angle brackets denote a time average over 1 ms (much longer than the turbulent fluctuation lifetime and shorter than anomalous transport time scales), and B is the toroidal magnetic field. The signals are connected to 500 kHz digitizer cards. The fluctuating quantities are analysed using standard techniques [6, 18] with a bandwidth of $1 < f < 250$ kHz and neglecting temperature fluctuations.

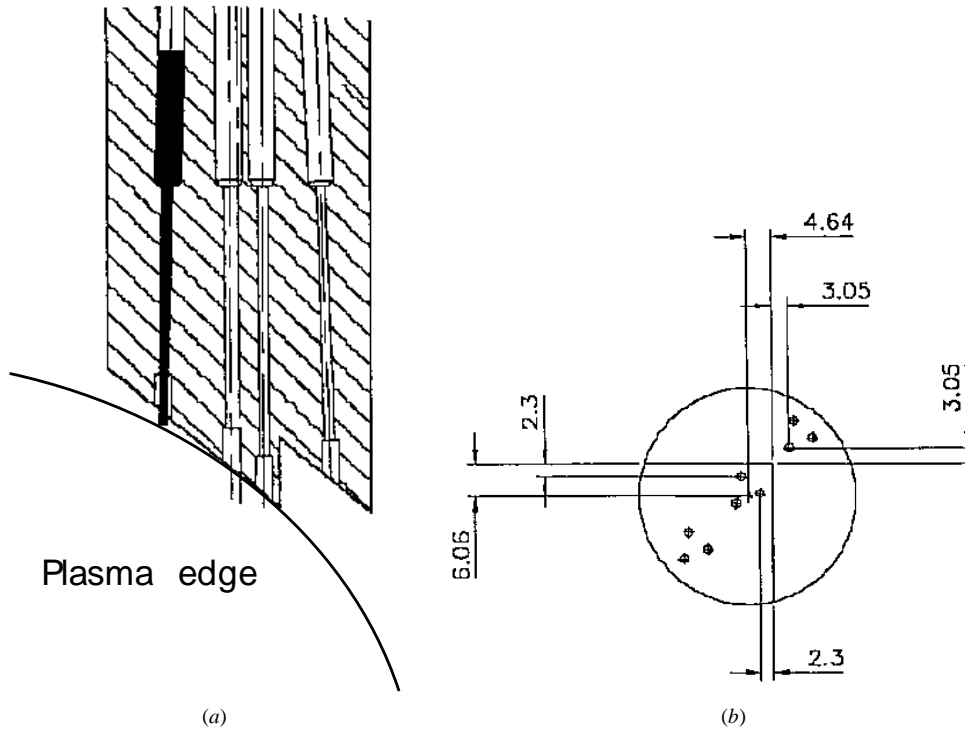


Figure 1. Schematic view of the nine-pin probe head used for turbulence measurements in the JET tokamak, showing (a) how the probe surface matches the plasma shape, and (b) a top view of the tips. The distances are in millimetres.

3. Radial profile of the fluctuating quantities and turbulent flux

The general characteristics of the turbulence were analysed in the limiter phase of two shots: 45783 ($B_T = 2.6$ T, $I_p = 2.2$ MA and $\bar{n}_e = 2 \times 10^{19}$ m $^{-3}$) and 45798 ($B_T = 2.4$ T, $I_p = 2$ MA and $\bar{n}_e = 1.5 \times 10^{19}$ m $^{-3}$). The position of the last closed flux surface (LCFS) is determined by the equilibrium code EFIT [19] using the plasma profiles and flux loops distributed about the vacuum vessel. The accuracy of the EFIT calculation is about ± 10 mm, at the outer midplane of JET. The fluctuating quantities are plotted against the distance from the LCFS mapped to the outer mid-plane (shown in figures 2 and 3).

The ion saturation current increases and the floating voltage goes to more negative values as the probe moves into the plasma edge (figures 2(a) and 2(b) respectively). The normalized ion saturation current fluctuation levels are shown in figure 2(c); this quantity approaches 0.6 near the wall and decreases across the SOL as the probe moves towards the main plasma. The fluctuation level reaches about 10–20% at the innermost probe position. Similar results have been obtained in other devices [20, 21]. The poloidal wave number is in the range of $k_\theta = -(0.5-1)$ cm $^{-1}$ in the SOL and changes sign as the probe approaches the edge of the main plasma (1 cm inside the nominal separatrix position), as can be observed in figure 2(d).

The poloidal phase velocity of fluctuations changes sign as the probe moves into the edge of the main plasma. The radial position where this change occurs is called the velocity shear layer (VSL) [22] (figure 3(b)). As observed in other machines [3], the propagation of the fluctuations is in the ion diamagnetic direction at the SOL region, but it reverses to the electron

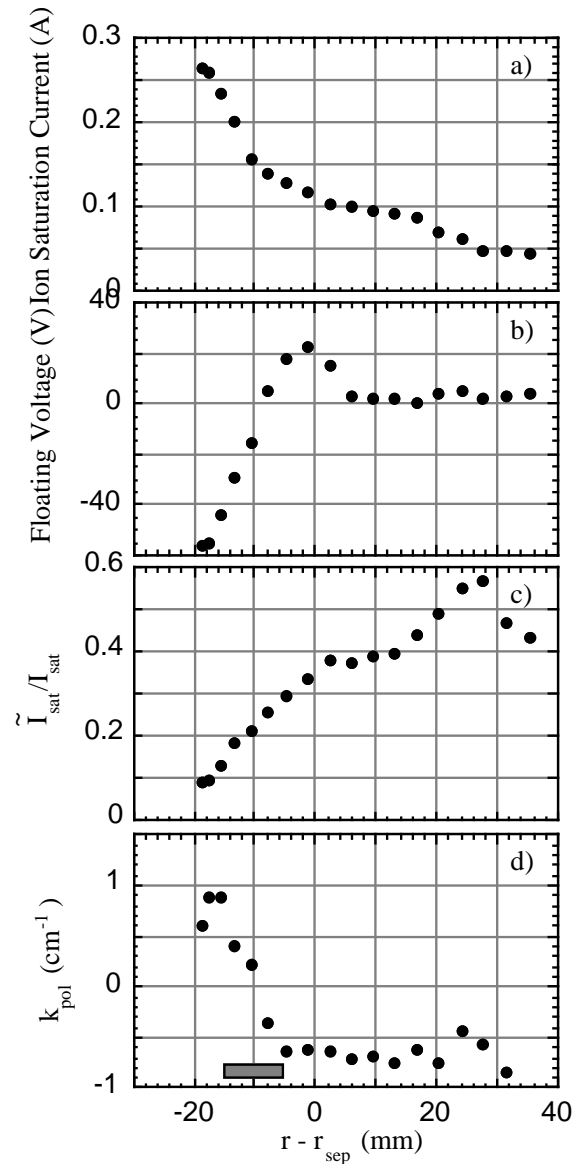


Figure 2. Ion saturation current (a), floating voltage (b), normalized fluctuation of the ion saturation current (c) and poloidal wave number (d) versus distance from the separatrix position, positive values being in the SOL and negative inside the LCFS. The position of the LCFS was estimated by magnetic codes. The shaded region shows the velocity shear layer location.

diamagnetic direction going to the edge of the main plasma. The location of the VSL does not coincide with the peak of the plasma potential where the radial electric field $E_r = -(dV_p/dr)$ changes its direction from outward to inward. In limiter discharges, the radial location where the radial electric field changes sign is localized at the maximum value of the floating potential, because the electron temperature slowly varies with radius at this plasma region [23]. Inside the LCFS, the main contribution to the electron drift velocity, $v_e = (T_e/eB)(1/L_n + 1/L_T) - E_r/B$, (where L_n and L_T are density and temperature scale length) is the radial electric field because

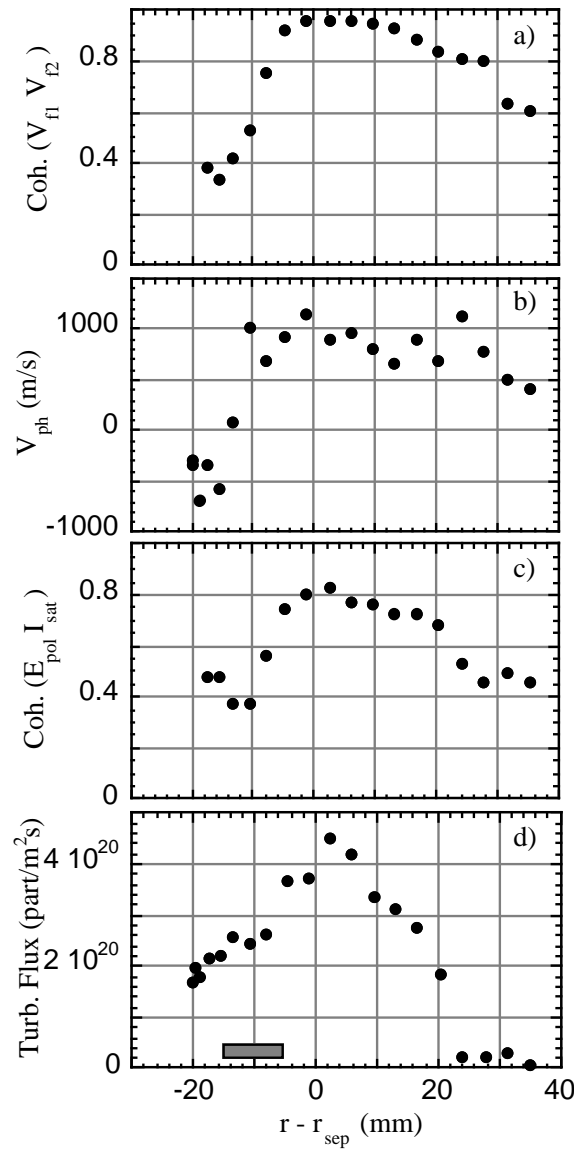


Figure 3. Coherence between two floating voltages, with a poloidal distance of 5 mm (a), poloidal phase velocity of the fluctuations (b), coherence between poloidal electric field and ion saturation current (c), and turbulent particle transport (d) versus distance from the separatrix position, for the same discharge as in figure 2. The shaded region also shows the velocity shear layer location.

the density and electron temperature gradients slowly change with radius, and it is found to be $v_e \approx v_{E \times B} \approx 2 \times 10^3 \text{ m s}^{-1}$, which is of the order of the poloidal phase velocity of the fluctuations $v_{ph} \approx 10^3 \text{ m s}^{-1}$. Traditionally the shear layer location has been used as a convenient point of reference for the comparison of the turbulence structure in different devices. In the present experiments (see figure 3) the velocity shear location is about 1 cm inside the LCFS estimated from the magnetic codes, and it is localized close to the maximum variation of the radial electric field.

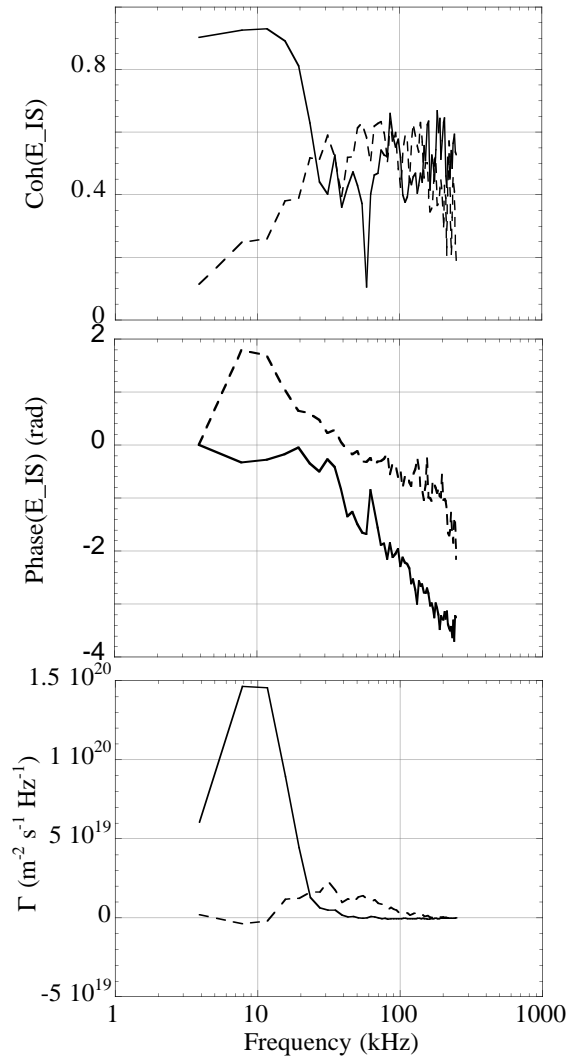


Figure 4. Coherence and phase between poloidal electric field and ion saturation current, and turbulent flux, versus frequency. The full curve corresponds to the probe position at LCFS and the dashed curve to a position 1 cm into the edge of the main plasma.

Significant poloidal coherence between two floating voltages (\tilde{V}_{f1} \tilde{V}_{f2}) (5 mm poloidally apart) and between poloidal electric field and ion saturation current ($\tilde{E}_\theta \tilde{I}_s$) has been observed in the whole radial profile, but it decreases as the probe moves into the edge of the main plasma (figures 3(a) and 3(c) respectively). This effect has also been observed in other tokamaks [20], and has been explained in terms of the influence of radially varying $E \times B$ poloidal flows in the cross correlation of fluctuations and/or by a decorrelation in the fluctuations by the effect of the velocity shear layer [24].

The radial profile of the time averaged turbulent flux is shown in figure 3(d). Taking the maximum of the flux as a reference, the turbulent particle flux must decrease as one moves into the SOL simply because of the parallel transport which drives the particles to the limiter surface. On the other hand, the turbulent flux has to decrease going into the edge of the main

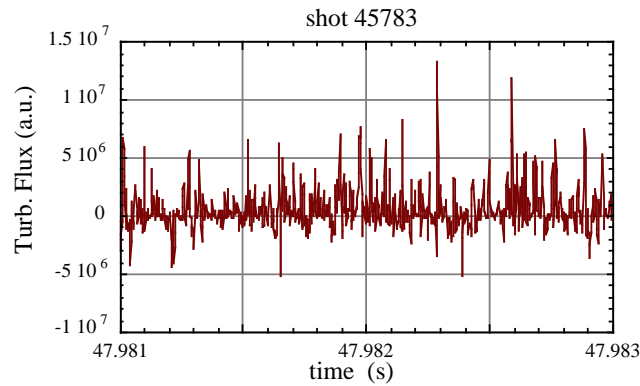


Figure 5. Time evolution of the $E \times B$ turbulent particle flux at the innermost position reached by the probe (2 cm inside the LCFS) in the limiter phase of the shot 45783.

plasma because of the continuity of the radial particle fluxes across closed flux surfaces and the decrease of the ionization source. This behaviour is indeed observed in the limiter discharges and the maximum appears at the position of the LCFS calculated with the magnetic codes, but it does not coincide with the velocity shear location. The width of the banana orbits for these plasma conditions is about 5–10 mm, which is in the range of the distance between the VSL and the LCFS. Therefore, this observation may be an indication that banana orbits are responsible for the formation of the radial electric fields at the edge of the plasma in JET limiter phases.

Figures 4(a) and 4(b) show the coherency and phase between poloidal electric field and ion saturation current in a frequency resolved plot (in a frequency band $2 < f < 250$ kHz), at two different radial positions (at the LCFS and 1 cm inside the LCFS calculated by magnetic codes). These two quantities are critical for the estimation of the radial particle turbulent flux. The frequency resolved turbulent flux is shown in figure 4(c) at two different radial positions (at the LCFS and 1 cm inside the LCFS calculated by magnetic codes). The contribution of the low frequency range dominates the turbulent flux at the LCFS. This remains true for the whole radial range of the SOL. In contrast, high frequencies become significant as one goes into the edge of the main plasma, while turbulent transport at low frequency is almost negligible in this region. Details about the shape of the fluctuation and transport spectra will be given in section 5.

Figure 5 shows the time evolution of the turbulent flux, measured in the innermost position reached by the probe, 2 cm inside the magnetic LCFS, in shot 45783. Positive values correspond to the outward particle flux and negative values to inward flux. Although the mean value is positive (outward particle flux), part of the flux is directed into the plasma. It is also observed in figure 5 that the turbulent particle fluxes come in bursts: outward pulses of a very short duration, irregularly distributed in time, make the most important contribution to the total particle flux. Analysis of the radial correlation length has been carried out and a high turbulent flux radial coherence has been observed for these specific shots.

The observation that the turbulent flux comes in bursts seems to be common to most devices [25, 26]. This result could be an indication of transport close to instability thresholds (i.e. SOC) [27]. These models incorporate a critical parameter that controls the behaviour of the system. When this parameter is close to or higher than a critical value the system relaxes suddenly by fast processes that take the parameter to a sub-critical value. One example of

these models is the sand pile model where the critical parameter is the slope of the pile and the relaxation processes are the particle avalanches. Time evolution of such avalanches is rather similar to the observed turbulent particle fluxes in fusion devices. From a random superposition of avalanches one would expect, in these SOC models, to observe a $1/f$ spectral dependence of the frequency spectrum where the fluxes are relevant. This point will be discussed in section 5.

4. Comparison between turbulent particle transport and global particle/energy confinement time

The perpendicular diffusion coefficient, D_{perp} , is estimated subject to the assumption that the transport is dominated by turbulence and using the expression $D_{\text{perp}} = \langle \tilde{I}_s \tilde{E}_\theta \rangle \lambda_n / B_T I_s$. From the measured plasma profiles (see figure 2(a)), the SOL density decay length (λ_n) is 1 cm mapped to the outer mid-plane of the plasma, and therefore the value obtained for these discharges is $D_{\text{perp}} = 1.5 \text{ m}^2 \text{ s}^{-1}$, at the LCFS.

The SOL input power, computed as the difference between the plasma input power and the radiated power, is about 1 MW for these discharges. The convective power associated with turbulent transport is $P_{\text{conv}} = 3/2 k_b (T_e + T_i) \Gamma_{\text{turb}} A_{\text{SOL}}$, where P_{conv} is the total convective power to the SOL, T_e and T_i are the separatrix electron and ion temperature (about 40 eV, $T_e = T_i$ is assumed), Γ_{turb} is the turbulent particle flux measured by Langmuir probes at the LCFS ($4 \times 10^{20} \text{ m}^{-2} \text{ s}^{-1}$), and A_{SOL} is the SOL area (about 100 m^2). Then, assuming poloidal symmetry, the obtained convective power is $P_{\text{conv}} = 0.6\text{--}0.8 \text{ MW}$. This is indeed somewhat larger than the typical convective losses for L-mode discharges in JET, which can account for up to 30% [28] of the energy losses, but it is within the error in the assumptions used in the present derivation. Therefore, the total power carried by the turbulent particle flux measured by Langmuir probes is not in contradiction of the SOL total input power.

However, it should be noted that poloidal asymmetry in turbulent transport probably exists at the edge of limiter plasmas. In the CCT tokamak [29] the poloidal asymmetries are found to be quite significant, with the maximum of the turbulent fluxes at the top and bottom of the plasma, while they are significantly reduced at both inner and outer mid-planes.

Turbulent particle flux measurements have also been carried out in X-point configuration plasmas. The turbulent flux is about one order of magnitude larger than in limiter magnetic configurations (for similar plasma conditions), in contradiction of the global particle and energy confinement time of the plasma. The argument of poloidal asymmetries that was used in DIII-D to explain the high level of particle fluxes measured at the outer mid-plane [13] does not apply here because the measurements are performed at the top of the machine. The high particle turbulent flux found in X-point plasmas could be related to the convective cell flows which may be present in the SOL of divertor plasmas. Studies are underway to clarify this issue.

5. Frequency ranges in the spectrum of plasma edge fluctuations and their relation to turbulent fluxes

In the experimental studies of plasma fluctuations it has been observed that there are several frequency ranges in the fluctuation power fall-off behaviour with different and well-defined decay indices. In [30] three regions are described. The lowest frequency part of the spectrum is found to be nearly independent of the frequency. The high-frequency part shows an asymptotic fall-off with decay indices close to -2 or even lower. There is also an intermediate frequency region that behaves like $1/f$. It is important to do this analysis in the plasma rest frame, i.e.

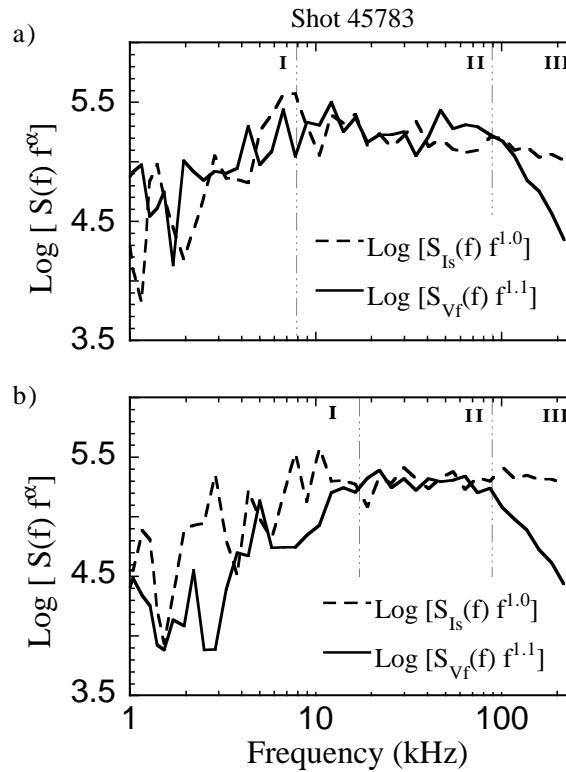


Figure 6. Spectra of the ion saturation current (dashed curve) and floating potential fluctuation (full curve) taken from 10 ms data sections at 1 cm inside the edge of the main plasma (a), and 2 cm inside the edge of the main plasma (b). The spectra $S(f)$ are multiplied by f^α to have a flat intermediate region and are plotted with an arbitrary offset.

at the point where the poloidal flow velocity is zero, in order to avoid the Doppler effect that modifies the spectral shape, as was pointed out in [29].

The sampling frequency is 500 kHz for the JET experiments analysed here, and the fluctuation record length used in the calculation of the spectrum is 5000 points. The phase velocity of the fluctuations is taken as an estimate of the poloidal flow velocity. A logarithmic binning of the spectrum [29] has been used in order to get a clear determination of the breaking or transition frequencies. After identifying the breakpoints a simple power function was fitted to the spectrum, such as $S(f) = Af^{-\alpha}$, where $S(f)$ is the power spectrum of the fluctuating signal, A is a constant and α is the decay index. Then, the power spectrum is multiplied by f^α and the resulting function is plotted. Using this method, the two frequency breakpoints and the corresponding three frequency regions can be identified.

This is illustrated in figure 6(a), where $S(f)f^\alpha$ is shown as a function of the frequency, as one moves into the edge of the main plasma. In this figure, $S(f)$ is the power spectrum of the floating potential and ion saturation current for the discharge 45783 at the velocity shear layer radial position. Figure 6 clearly shows that there is a fairly flat region between 10 kHz and 100 kHz for the first case (figure 6(a)) and between 20 kHz and 90 kHz for the second case (figure 6(b), which corresponds to 2 cm inside the nominal separatrix position). This indicates that the power law is an accurate fit in these frequency regions. However, it is more difficult to get a clear determination of the position of the frequency breakpoints. In particular,

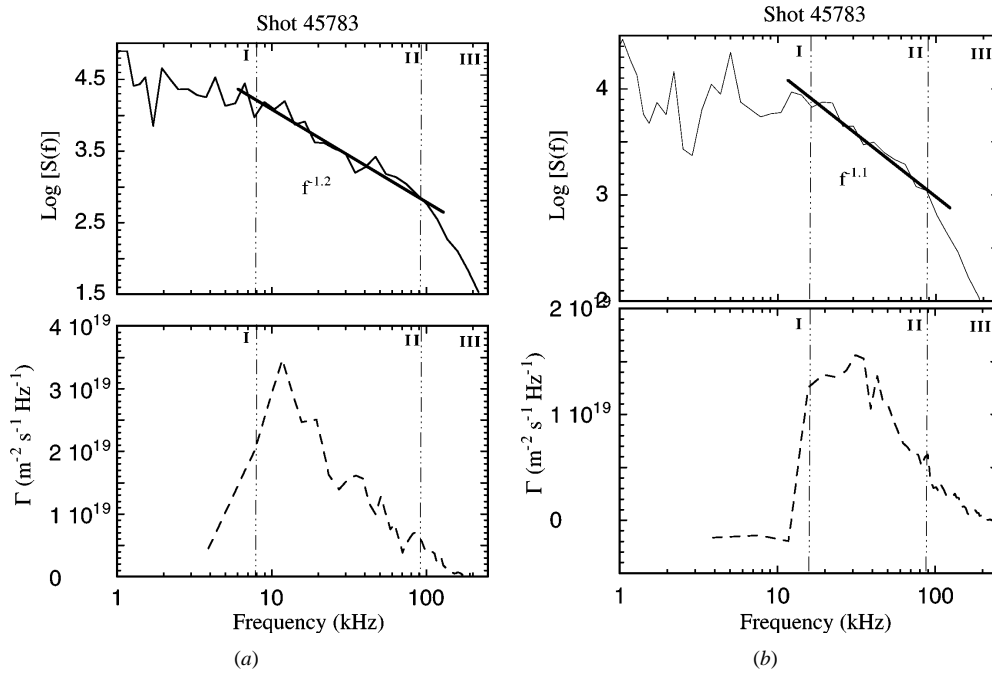


Figure 7. Floating potential fluctuation spectra corresponding to the previous data. Also in the plot is the spectral flux function for the same discharge.

the possible presence of MHD activity, plasma column drifts, motion of the probes, etc could often distort the fluctuation spectra.

Figures 7(a) and 7(b) show the original power spectra, $S(f)$ and the corresponding frequency resolved particle flux for two different radial positions (1 cm and 2 cm respectively inside the LCFS as computed by magnetic codes). The frequency range with power decay close to $1/f$ plays the most important role in plasma transport. This correlation between the $1/f$ fluctuation range and transport dynamics could be an indication of transport close to instability thresholds.

6. Conclusions

A systematic analysis of the turbulence characteristics has been carried out for the boundary of JET limiter plasmas. In general, the characteristics of turbulence in JET limiter plasmas are similar to those observed in most of the fusion devices.

A reversal in the poloidal phase velocity (shear layer) has been observed in the plasma edge region. The radial location of the shear layer is shifted by about 1 cm (of the order of the banana width orbit) with respect to the radial position where the $E \times B$ turbulent flux reaches its maximum value.

The perpendicular diffusion coefficient deduced from turbulent particle transport is about $1.5 \text{ m}^2 \text{ s}^{-1}$ at the last closed flux surface in JET ohmic limiter plasmas with $B_T = 2.4\text{--}2.6 \text{ T}$, $I_p = 2\text{--}2.2 \text{ MA}$ and $\bar{n}_e = 1.5\text{--}2 \times 10^{19} \text{ m}^{-3}$. The total turbulent particle transport can account for the global particle/energy confinement time in limiter plasmas. The turbulent transport time evolution shows bursts of particle flux, which might be an indication of transport close to instability thresholds.

The obtained turbulent flux in X-point plasmas is about one order of magnitude larger than in the limiter magnetic configuration (for similar plasma conditions), which is in contradiction of the global particle and energy confinement time of the plasma. The high turbulent particle flux found in X-point plasmas could be related to the convective cell flows which may be present in the SOL of divertor plasmas. Studies are underway to clarify this issue.

Analysis of the plasma edge ion saturation current and floating potential fluctuation spectra in several limiter shots shows the existence of three distinct fluctuation ranges. In each of these ranges, and in the absence of MHD activity, the spectrum is well described by an algebraic function. The most interesting region is the intermediate frequency range. In this range, the spectral decay index is around -1 when the Doppler shift effects induced by plasma velocity have been taken into account. This frequency range corresponds to the maximum of the turbulent particle flux.

Acknowledgments

This work was funded jointly by the UK Department of Trade and Industry and EURATOM.

References

- [1] Zweben S J, Liewer P C and Gould R W 1982 *J. Nucl. Mater.* **111–112** 39
- [2] Ritz C P, Bengtson R D, Levison S J and Powers E J 1984 *Phys. Fluids* **27** 2956
- [3] Wooton A J, Carreras B A, Matsumoto H *et al* 1990 *Phys. Fluids* **12** 2879
- [4] Levison S J *et al* 1984 *Nucl. Fusion* **24** 527
- [5] Wooton A J *et al* 1986 Electrostatic fluctuations and transport in the edge of the ISX-B tokamak *Oak Ridge Report ORNL/TM-9305*, Oak Ridge National Laboratory, Oak Ridge, TN
- [6] Robinson D C 1987 Turbulence and anomalous transport in magnetized plasmas *Editions de Physique* ed D Gresillon and M A Dubois (Orsay) p 21
- [7] Mantica P *et al* 1989 *Proc. 16th European Physical Society Conf. on Controlled Fusion and Plasma Physics (Venice)* vol 13B (Geneva: European Physical Society) p 967
- [8] Thomsen H *et al* 1999 *Proc. 26th European Physical Society Conf. on Controlled Fusion and Plasma Physics (Maastricht) Europhysics Conference Abstracts* (Geneva: European Physical Society) vol 23J p 1541
- [9] Antoni V *et al* 1998 *Phys. Rev. Lett.* **80** 4185
- [10] Hidalgo C 1995 *Plasma Phys. Control. Fusion* **37** A53–A67
- [11] Moyer R A, Watkins J G, Conn R W *et al* 1992 *J. Nucl. Mater.* **196–198** 854–9
- [12] Moyer R A, Cuthbertson J W *et al* 1997 *J. Nucl. Mater.* **241–243** 633–8
- [13] Carreras B A, Milligen B v, Pedrosa M A *et al* 1998 *Phys. Rev. Lett.* **80** 4438–41
- [14] Pedrosa M A, Hidalgo C, Carreras B A *et al* 1999 *Phys. Rev. Lett.* to be published
- [15] Keilhacker M and the JET Team 1999 *Nucl. Fusion* **39** 209
- [16] García-Cortés I *et al* 1999 *Proc. 26th European Physical Society Conf. on Controlled Fusion and Plasma Physics (Maastricht) Europhysics Conference Abstracts* (Geneva: European Physical Society) vol 23J p 373
- [17] Powers E J 1974 *Nucl. Fusion* **14** 749–52
- [18] Beall J, Kim Y C and Powers E J 1982 *J. Appl. Phys.* **53** 3933
- [19] O'Brien D P *et al* 1992 *Nucl. Fusion* **32** 1351
- [20] García-Cortés I *et al* 1992 *Phys. Fluids B* **4** 4007–11
- [21] Giannone L, Balbín R, Niedermeyer H *et al* 1994 *Phys. Plasmas* **1** 3614
- [22] Ritz C P, Rhodes T L, Lin H *et al* 1991 *Proc. 13th Conf. Plasma Physics and Controlled Nuclear Fusion Research (Washington DC)* vol 2 (Vienna: IAEA) p 589
- [23] Erents S K, Tagle J A, McCracken G M *et al* 1988 *Nucl. Fusion* **28** 1209
- [24] Hidalgo C, Harris J H, Uckan T *et al* 1991 *Nucl. Fusion* **31** 1471
- [25] Endler M, Niedermeyer H, Giannone L *et al* 1995 *Nucl. Fusion* **35** 1307
- [26] Sanchez E 1996 *Transport, Chaos and Plasma Physics 2. Equ. Turbulence Plasma (Université de Provence; 10–22 July, 1995)* (Singapore: World Scientific)
- [27] Bak P, Tang C and Wiesenfeld K 1987 *Phys. Rev. Lett.* **59** 381–4

- [28] Tibone F *et al* 1989 *Proc. 16th European Physical Society Conf. on Controlled Fusion and Plasma Physics (Venice)* vol 13B (Geneva: European Physical Society) p 282
- [29] Tynan G R 1996 *Transport, Chaos and Plasma Physics 2. Equ. Turbulence Plasma (Université de Provence, IMT Marseille, 10–22 July, 1995)* (Singapore: World Scientific)
- [30] Carreras B A *et al* 1999 *Phys. Plasmas* to be published